

## MIT Open Access Articles

*Reactive ion etching: Optimized diamond membrane fabrication for transmission electron microscopy*

The MIT Faculty has made this article openly available. **Please share** how this access benefits you. Your story matters.

**Citation:** Li, Luozhou, Matthew Trusheim, Ophir Gaathon, Kim Kisslinger, Ching-Jung Cheng, Ming Lu, Dong Su, et al. "Reactive Ion Etching: Optimized Diamond Membrane Fabrication for Transmission Electron Microscopy." J. Vac. Sci. Technol. B 31, no. 6 (2013): 06FF01. © 2013 American Vacuum Society

**As Published:** <http://dx.doi.org/10.1116/1.4813559>

**Publisher:** American Vacuum Society (AVS)

**Persistent URL:** <http://hdl.handle.net/1721.1/86147>

**Version:** Final published version: final published article, as it appeared in a journal, conference proceedings, or other formally published context

**Terms of Use:** Article is made available in accordance with the publisher's policy and may be subject to US copyright law. Please refer to the publisher's site for terms of use.



## Reactive ion etching: Optimized diamond membrane fabrication for transmission electron microscopy

Luozhou Li, Matthew Trusheim, Ophir Gaathon, Kim Kisslinger, Ching-Jung Cheng et al.

Citation: *J. Vac. Sci. Technol. B* 31, 06FF01 (2013); doi: 10.1116/1.4813559

View online: <http://dx.doi.org/10.1116/1.4813559>

View Table of Contents: <http://avspublications.org/resource/1/JVTBD9/v31/i6>

Published by the AVS: Science & Technology of Materials, Interfaces, and Processing

### Related Articles

Feature profile evolution during shallow trench isolation etching in chlorine-based plasmas. III. The effect of oxygen addition

*J. Vac. Sci. Technol. B* 31, 042201 (2013)

Stability and etching of titanium oxynitride films in hydrogen microwave plasma

*J. Vac. Sci. Technol. A* 31, 041304 (2013)

Selective etching of TiN over TaN and vice versa in chlorine-containing plasmas

*J. Vac. Sci. Technol. A* 31, 031305 (2013)

Wet chemical etching process for wafer scale isolation and interconnection of GaSb based device layers grown on GaAs substrates

*J. Vac. Sci. Technol. B* 31, 031204 (2013)

Fabrication of 3D charged particle trap using through-silicon vias etched by deep reactive ion etching

*J. Vac. Sci. Technol. B* 31, 032001 (2013)

### Additional information on *J. Vac. Sci. Technol. B*

Journal Homepage: <http://avspublications.org/jvstb>

Journal Information: [http://avspublications.org/jvstb/about/about\\_the\\_journal](http://avspublications.org/jvstb/about/about_the_journal)


Top downloads: [http://avspublications.org/jvstb/top\\_20\\_most\\_downloaded](http://avspublications.org/jvstb/top_20_most_downloaded)

Information for Authors: [http://avspublications.org/jvstb/authors/information\\_for\\_contributors](http://avspublications.org/jvstb/authors/information_for_contributors)

## ADVERTISEMENT


# Instruments for advanced science

#### Gas Analysis



- dynamic measurement of reaction gas streams
- catalysis and thermal analysis
- molecular beam studies
- dissolved species probes
- fermentation, environmental and ecological studies

#### Surface Science



- UHV TPD
- SIMS
- end point detection in ion beam etch
- elemental imaging - surface mapping

#### Plasma Diagnostics



- plasma source characterization
- etch and deposition process reaction kinetic studies
- analysis of neutral and radical species

#### Vacuum Analysis



- partial pressure measurement and control of process gases
- reactive sputter process control
- vacuum diagnostics
- vacuum coating process monitoring

contact Hiden Analytical for further details

## HIDEN ANALYTICAL

[info@hideninc.com](mailto:info@hideninc.com)  
[www.HidenAnalytical.com](http://www.HidenAnalytical.com)  
CLICK to view our product catalogue

# Reactive ion etching: Optimized diamond membrane fabrication for transmission electron microscopy

Luozhou Li<sup>a)</sup>

*Department of Electrical Engineering, Columbia University, New York, New York 10027*

Matthew Trusheim and Ophir Gaathon

*Department of Applied Physics and Applied Mathematics, Columbia University, New York, New York 10027 and Department of Electrical Engineering and Computer Science, Massachusetts Institute of Technology, Cambridge, Massachusetts 02139*

Kim Kisslinger, Ching-Jung Cheng, Ming Lu, and Dong Su

*Center for Functional Nanomaterials, Brookhaven National Laboratory, Upton, New York 11973*

Xinwen Yao and Hsu-Cheng Huang

*Department of Electrical Engineering, Columbia University, New York, New York 10027*

Igal Bayn

*Department of Electrical Engineering and Computer Science, Massachusetts Institute of Technology, Cambridge, Massachusetts 02139*

Abraham Wolcott

*Department of Chemistry, Columbia University, New York, New York 10027*

Richard M. Osgood, Jr.

*Department of Electrical Engineering and Department of Applied Physics and Applied Mathematics, Columbia University, New York, New York 10027*

Dirk Englund<sup>b)</sup>

*Department of Electrical Engineering and Computer Science, Massachusetts Institute of Technology, Cambridge, Massachusetts 02139*

(Received 15 May 2013; accepted 23 June 2013; published 15 July 2013)

Commonly used preparation method for thin diamond membranes by focused ion beam (FIB) techniques results in surface damage. Here, the authors introduce an alternative method based on reactive ion etching (RIE). To compare these methods, cross-sectional samples are produced in single crystal diamond, a material that has generated growing interest for a variety of applications. The samples are examined by Raman spectroscopy and high-resolution transmission electron microscopy (TEM). Raman spectra indicate that the crystalline structure of the RIE-processed diamond is preserved, while the FIB-processed diamond membrane has a broad-background  $sp^2$  feature. Atomic-resolution TEM imaging demonstrates that the RIE-based process produces no detectable damage, while the FIB-processed sample has an amorphous carbon layer of about 11 nm thick. These findings show that the RIE-based process allows the production of diamond TEM samples with reduced near-surface damage and can thus enable direct examination of growth defects and crystallographic damage induced by processes such as ion implantation and bombardment. © 2013 American Vacuum Society. [<http://dx.doi.org/10.1116/1.4813559>]

## I. INTRODUCTION

Sample preparation of bulk materials for transmission electron microscopy (TEM) has been a topic of extended studies, but important challenges persist. There are several commonly used techniques for preparing cross-sectional samples, such as tripod polishing, cleaving, argon ion milling, and focused ion beam (FIB).<sup>1–3</sup> Of these techniques, FIB is the most controllable method to generate electron-transparent membranes with site-specific positional accuracy on the sub-micron scale.<sup>4–6</sup> Unfortunately, this method also results in extensive surface amorphitization, which can present challenges for TEM studies with atomic resolution.<sup>2,7,8</sup>

The exceptional properties of diamond, including its 5.5 eV electronic bandgap,<sup>9</sup> high carrier mobility (boron doping),<sup>10</sup> elevated breakdown electric field properties,<sup>11</sup> excellent thermal conductivity,<sup>12</sup> and biocompatibility,<sup>13</sup> make it an attractive choice for applications in electronic, photonic, and sensing devices.<sup>14–16</sup> In addition to these well-known properties, defect color centers in diamond have appealing characteristics for quantum information technologies.<sup>17–21</sup> For example, the negatively charged nitrogen-vacancy center (NVC) in diamond is one of the most promising candidates for solid-state qubit due to its fast optical initialization, readout, and long spin-coherence time at room temperature.<sup>22</sup> Ion-implantation techniques are widely used to generate defect color centers<sup>23–26</sup> and to create diamond nano-structures.<sup>27–30</sup> Diamond damage due to ion implantation has been examined with TEM using

<sup>a)</sup>Electronic mail: ll2670@columbia.edu

<sup>b)</sup>Electronic mail: englund@mit.edu

FIB-produced membrane samples.<sup>31–33</sup> FIB-based techniques rely on physical bombardment of the sample surface by high-energy gallium ions. These methods result in near-surface damage of the diamond,<sup>34,35</sup> as they do in many other materials. Such damaged layers increase background scattering and obscures the proper imaging of crystal-lattice fringes and of individual atoms. Improvements in membrane preparation-methods are needed for direct examination of growth defects and crystallographic damage in diamond.

In this paper, we use diamond as a particularly challenging and important material to demonstrate a low-damage TEM-sample-preparation method based on reactive ion etching (RIE); RIE has recently been applied to diamond nanofabrication. It uses a reactive plasma, which is generated under low pressure by a microwave field and at low energy, to chemically etch the diamond. Reactive ions from the plasma react with the diamond surface and remove material gradually. RIE ions are known to have a relatively minimal adverse effect on optical properties;<sup>18,19</sup> also RIE is used to manipulate the charge state of NVC by changing surface termination after ion milling.<sup>36–38</sup> Furthermore, our previous spin-echo experiments in RIE-processed diamond membranes show negatively charged NVCs with spin-coherence times approaching 100  $\mu$ s;<sup>39</sup> these spin properties are consistent with those in the parent high-purity bulk diamond.

The creation of diamond thin membranes *with minimal process-induced damage* is not only important to improve the quality of fabricated nanostructures, but also to enable rigorous atomic-level investigation of other damage pathways in the diamond lattice, such as growth defects and radiation-induced damage (e.g., nitrogen implantation and helium bombardment). In this work, we fabricate thin diamond membranes for TEM studies using two ion-involved processes: the established FIB process<sup>33</sup> and our recently developed diamond RIE process.<sup>39</sup> The material properties of the resultant diamond membranes are studied by Raman spectroscopy and high-resolution transmission electron microscopy (HRTEM). Raman spectra indicate that the crystal-line structure of the RIE-processed diamond is preserved, while the FIB-processed diamond membrane has a broad-background  $sp^2$  feature. Atomic-resolution examination

shows that the RIE-based process produces no discernible damage and prevents the generation of amorphous carbon on the diamond surface.

## II. EXPERIMENT

In the experiments, type IIa single-crystal diamonds ( $3\text{ mm} \times 3\text{ mm} \times 300\text{ }\mu\text{m}$ ) were used (sourced from Element Six). Prior to any fabrication, the samples were exposed to a boiling 1:1:1 nitric:sulfuric:perchloric ( $\text{HNO}_3:\text{H}_2\text{SO}_4:\text{HClO}_4$ ) acid mixture. After surface cleaning, the samples were made via both FIB- and RIE-based processing. The FIB process used an FEI HELIOS Nanolab 600 Dual Beam (FIB/SEM) system, following a standard FIB lift-out technique.<sup>33</sup> Using a gallium-ion beam at 30 keV, two 6- $\mu$ m-deep trenches were milled into diamond, as shown in the inset image of Fig. 1(a). The vertical membrane was lifted out by an Omniprobe tungsten tip and moved onto an adjacent copper grid [Fig. 1(a)]. Figure 1(b) shows the membrane bonded to the grid by platinum deposition. At this point, the sample dimensions were  $10\text{ }\mu\text{m} \times 6\text{ }\mu\text{m} \times 1\text{ }\mu\text{m}$ . Further FIB milling at 30 keV and precision “polishing” at 2 keV were performed. These resulted in a diamond membrane attached to the grid with thickness of less than 100 nm in the region near the top section [denoted by black ellipse in Fig. 1(c)].

The RIE-based process used a JBX6300FS electron-beam lithography tool to pattern thin lines of hydrogen silsesquioxane (HSQ) that define the thickness of diamond membranes to be less than 200 nm. Low surface roughness of the resultant diamond membranes was achieved using HSQ as dry etching mask.<sup>19,40,41</sup> This mask pattern was transferred 2  $\mu$ m into the diamond using oxygen-plasma etching. To then transfer the mask pattern deeper, i.e., 10  $\mu$ m, into the diamond, we employed our previously developed etching method,<sup>42</sup> which alternates successively between plasma etching and mask deposition to produce vertical membranes [Fig. 2(a)]. Hundreds of membranes were thus created in parallel [Fig. 2(b)].

Following vertical etching, the diamond membranes were mechanically released from the bulk diamond while visually imaged with a long-working-distance stereoscope. A syringe

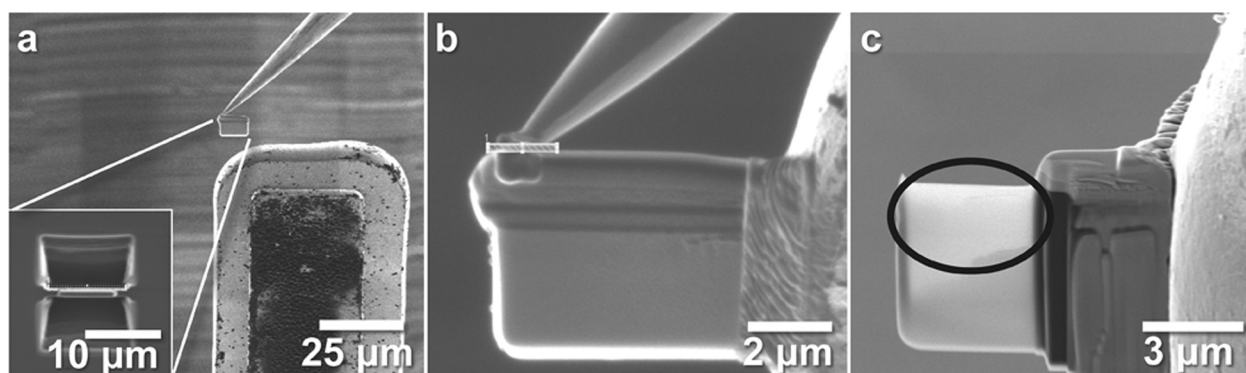


Fig. 1. Diamond membrane fabrication procedure using FIB. (a) Diamond membrane (side view), resulting from an FIB cut, is picked up from a bulk diamond sample and placed near a TEM grid. The inset shows a top view of the same diamond membrane after two 6- $\mu$ m-deep trenches were then milled into both sides of the membrane. (b) Expanded view of a sample bonded to a TEM grid. (c) Diamond sample after FIB thinning of a region, denoted by the black ellipse, to a thickness of less than 100 nm for HRTEM imaging.



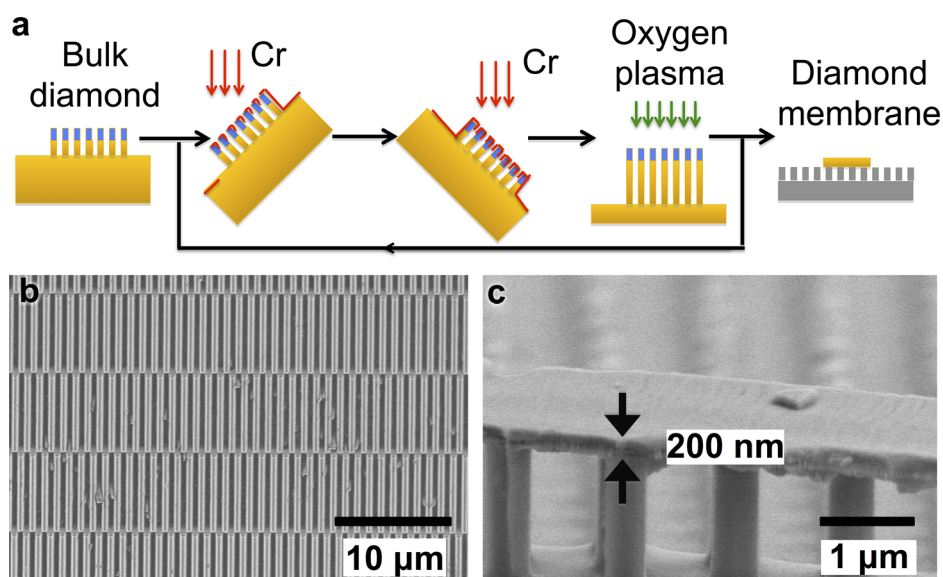


Fig. 2. (Color online) Diamond membrane fabrication procedure using RIE. (a) This process alternates between oxygen plasma etching and Cr mask deposition steps and results in a high-aspect-ratio diamond membrane. (b) Diamond membrane (top view) stands vertically on a bulk diamond sample before mechanical separation. (c) Diamond membrane (side view) is transferred onto a patterned silicon substrate.

needle mounted on a manual stage was used to mechanically separate specific rows of membranes from the diamond sample, leaving the remaining rows intact. Polydimethylsiloxane stamps were used to transfer these diamond membranes onto various substrates, such as glass cover slips, bulk silicon substrates, patterned silicon substrates [Fig. 2(c)], and TEM grids, for various applications. The versatility of the fabrication and transfer technique enables simple diamond-membrane preparation for spectroscopy and microscopy studies as well as device fabrication.

The Raman evaluation of these samples was performed after they were transferred onto a glass cover slip. Both FIB- and RIE-produced membrane samples were excited with a 5 mW 532 nm continuous-wave diode-pumped solid-state laser focused to a diffraction-limited spot size of 300 nm using a commercial confocal microscope [Zeiss Axio Observer, EC Epiplan-Neofluar Objective ( $\times 100$  NA = 0.9)]. The Raman spectra were acquired with a grating spectrometer. Both samples were also imaged with a JEOL JEM2100F, high-resolution analytical transmission electron microscope at 200 kV. *In-situ* energy dispersive x-ray spectra and electron diffraction patterns were used to identify the orientation and crystallinity of the thin diamond membranes.

### III. RESULTS AND DISCUSSION

Diamond has a single Raman first-order phonon mode at the center of the Brillouin zone with  $T_{2g}$  symmetry; this  $\Gamma$  phonon mode is due to interpenetrating fcc groups. The presence of this sharp Raman line allows diamond to be identified, even in the presence of a graphitic carbon background.<sup>42,43</sup> Visible-Raman spectroscopy is 50–250 times more sensitive to  $sp^2$ -hybridized carbon than  $sp^3$ -hybridized carbon and is qualitatively very robust in examining carbon species with various bonding geometries.<sup>44–46</sup> Figure 3 shows Raman data from RIE and FIB-produced

diamond membranes. Notably, the Raman spectrum from the RIE-processed diamond has only the  $\Gamma$  phonon mode at  $\sim 1332$   $cm^{-1}$ , with no other detectable  $sp^2$  species. This single-feature spectrum indicates that the crystalline structure of the RIE-processed diamond is preserved, and that graphitization and amorphitization are not occurring. In contrast, the FIB-processed diamond membrane shows a broad-background Raman feature most likely due to D and G bands of  $sp^2$  hybridized carbon centered at  $\sim 1330$  and  $1580$   $cm^{-1}$ , respectively.<sup>46</sup> This result is consistent with a previous report on FIB-generated diamond photonic structures.<sup>20</sup> The Raman spectrum indicates that  $sp^2$ -hybridized species form on the diamond during the FIB processing. This material consists of a combination of graphitized carbon and amorphous carbon species.<sup>47</sup>

The FIB-processed membrane is shown in a low-resolution TEM image with a selected-area electron diffraction (SAED) pattern of the single-crystal membrane [Fig. 4(a) and inset]. This pattern exhibits distinct spots indexed to the (100) and (110) crystal facets. A faint glow, or “halo” corresponding to an amorphous carbon surface, is visible.

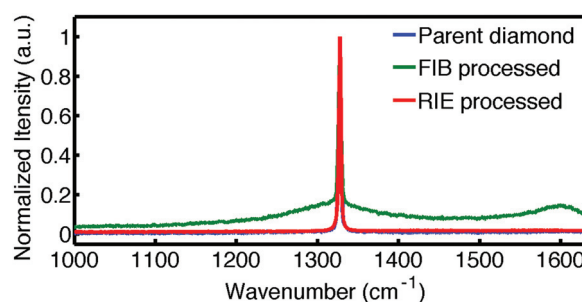


Fig. 3. (Color) Raman spectra from a pristine CVD diamond (curve shown in blue), FIB-processed diamond (curve shown in green), and RIE-processed diamond. FIB-processed diamond shows a broad-background Raman feature surrounding the Raman line.

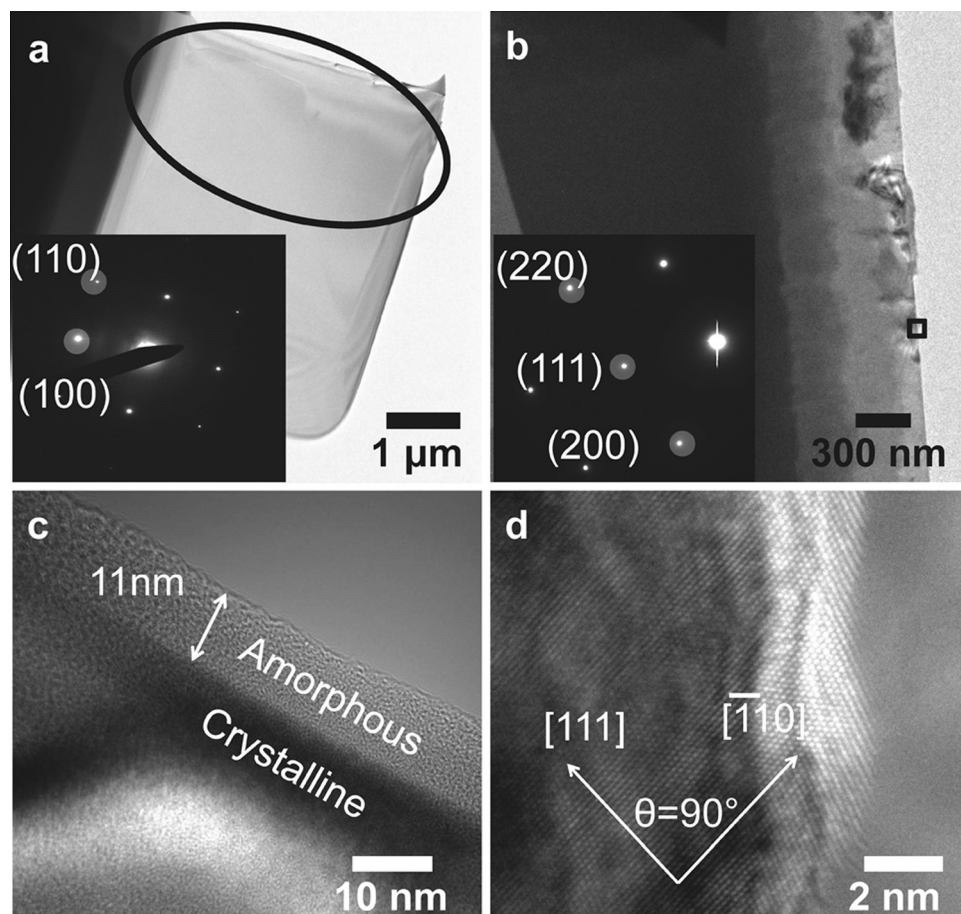


FIG. 4. TEM investigation of FIB- and RIE-processed diamond membranes. Low-magnification TEM images are taken from (a) FIB- and (b) RIE-processed diamond membranes with electron diffraction patterns (inset). HRTEM images are taken from (c) FIB- and (d) RIE-processed diamond membranes. (c) is the expanded view of the edge of black ellipse region in (a) to show the near-surface interface between amorphous and crystalline diamond. (d) is the expanded view of the black rectangular region of (b) to show diamond crystal without any visible damage with atomic resolution.

Correspondingly, the SAED pattern allows us to know that the zone-axis is along the  $[100]$  direction, and that the FIB-process direction was parallel to  $[100]$ . In contrast, the diffraction pattern of RIE-processed diamond membrane given in the inset of Fig. 4(b) shows diffraction spots without the halo corresponding to amorphous material. The diffraction spots are indexed to the  $(111)$ ,  $(200)$ , and  $(220)$  crystal facets. Since the  $[110]$  zone-axis is observed in the SAED, our RIE sample was prepared by cutting parallel to the  $(110)$  plane. The  $(110)$  plane has the densest number of atoms per facet area with  $\sim 22$  atoms/nm<sup>2</sup>. This difference in atomic planes is due to the different spatial orientation of the diamond “cuts.”

In this study, the FIB-processed membrane is slightly thinner than the RIE-produced membrane, but its TEM image lacks atomic resolution due to carbon contamination. The HSQ mask is able to produce sub-20-nm lines with RIE,<sup>48</sup> which makes its use possible for fabrication of ultrathin diamond membranes. We did not try to pursue the lower-thickness limit of RIE-produced membranes since we had already obtained HRTEM images from the edges of both samples.

A HRTEM image of FIB-processed diamond sample is shown in Fig. 4(c). It clearly shows the damaged layer on the

edge of the FIB sample; the amorphous character of this layer is about 11 nm in width. Apparently, gallium-ion bombardment damaged the diamond lattice, as a result of implantation into the diamond surface region. The FIB process thus coated the surface with amorphous carbon.<sup>34,35</sup> The d-spacing between adjacent  $(100)$  lattice planes is 0.356 nm, and would be expected to be readily imaged by 200 keV electrons with a wavelength of 2.5 pm. But gallium atoms and other superfluous carbon species coated the surface of the diamond membrane, preventing the clear observation of the single-crystal diamond lattice.

Simulations of the FIB process with 30 keV gallium ions using a stopping and range of ions in matter (SRIM) Monte Carlo code<sup>49</sup> shows that the gallium ions have a penetration depth of 14.3 nm in diamond. However, these simulations do not take into account volumetric change in the diamonds surface region, which may affect the precision of the estimated ion penetration. In particular, the diamond surface would swell due to the effects of implanted gallium and the decreased density of carbon atoms from 3.515 to 1.8 g/cm<sup>3</sup> during full amorphization.<sup>35</sup> Bayn *et al.*<sup>50</sup> reported a  $\sim 20$  nm amorphous layer when FIB is performed with a beam energy of 30 keV. In that work, the layer thickness was measured by time of flight secondary ion mass spectrometry. Our

measurements of the amorphous layer thickness is smaller than both SRIM simulation and previous SIMS results due to a short “polishing” etch with 2 keV after 30 keV etch. This damaged diamond layer, including implanted gallium atoms, would also have an adverse effect on diamond optical-performance, i.e., such as lower cavity resonances of photonic crystal defect cavities;<sup>20,51,52</sup> this is always present using the FIB process.

The RIE-based method enabled atomic-resolution imaging of the membrane. Figure 4(b) shows contrast changes (dark → light) due to the etching process, which indicates that RIE-produced membrane has a tapered, thinner region at the edge. Individual atoms are resolved under high magnification, and the [111] and  $[\bar{1}10]$  directions are highlighted in Fig. 4(d), and produce an angle of 90°. Note that no amorphous layer or graphite layer is visible on this RIE-produced membrane. Both electron-diffraction pattern and HRTEM images indicate that the RIE process does not introduce any detectable damage (i.e., graphitization or amorphitization), even at atomic resolution. This result is consistent with the clean Raman-scattering measurements presented above. The membrane becomes thinner at the edge, and the increased electron transparency allows for enhanced imaging.

To explain the RIE-preparation result, first note that the bias voltage for oxygen plasma was measured to be  $\sim 250$  V, which sets the upper limit of the acceleration energy of generated ions. SRIM simulations show that at the above-mentioned voltage, oxygen ions penetrate 0.8 nm into the diamond, which is equivalent to  $\sim 2$  atomic layers of 100 ( $d = 0.356$  nm) and  $\sim 4$  atomic layers of 111 ( $d = 0.205$  nm). In addition, the RIE process is based on etching that involves both oxygen-mediated chemical reactions and ion bombardment. Thus, the shallow damage layer is removed during the RIE process by the chemical reaction of carbon and oxygen, leaving the diamond surface in the form of a mixed-stoichiometry of CO and CO<sub>2</sub> gas. This reaction allows for the etching process to eliminate graphite and amorphous carbon species accumulation.

Our study emphasizes the importance of nonperturbative techniques to generate TEM samples for TEM studies with atomic resolution. The need to understand growth defect and crystallographic damage will ultimately impact diamond devices based on NVCs for quantum computing and sensing applications.

#### IV. CONCLUSIONS

The RIE-based TEM sample preparation method, described here, is superior due to its combination of physical and chemical etching that results in minimal surface damage below the threshold of detection. FIB processing results in the generation of graphite and amorphous carbon on diamond as determined by Raman spectroscopy. FIB-processed diamond membranes also exhibit an amorphous carbon layer on the surface in HRTEM, which does not appear in that of RIE-processed membranes. The RIE-based process, allowing for atomic imaging, can be used to detect growth defect and crystallographic damage caused by ion implantation and

bombardment (e.g., N and He<sup>+</sup>). This process, demonstrated here on diamond, can be extended to wide range of materials that are anisotropically etched in plasma. Moreover, this process allows fabrication of multiple membranes in parallel, while the FIB is limited to serial sample production. These advantages make RIE processing preferable over FIB in TEM sample preparation.

#### ACKNOWLEDGMENTS

This work was supported by the U.S. Air Force Office of Scientific Research Quantum Memories MURI, PECASE, and Young Investigator Program (AFOSR Grant No. FA9550-11-1-0014, supervised by Gernot Pomrenke), and in part by the Defense Threat Reduction Agency, Basic Research Award #HDTRA1-11-1-0022 to Columbia University. Research was carried out in part at the Center for Functional Nanomaterials, Brookhaven National Laboratory, which was supported by the U.S. Department of Energy, Office of Basic Energy Sciences, under Contract No. DE-AC02-98CH10886. The authors would like to thank Mircea Cotlet, Aaron Stein, Fernando Camino, Hsin-hui Huang, and Sergio Allegri for their assistance in this work.

- <sup>1</sup>J. C. Bravman and R. Sinclair, *J. Electron Microsc. Tech.* **1**, 53 (1984).
- <sup>2</sup>J. P. McCaffrey, M. W. Phaneuf, and L. D. Madsen, *Ultramicroscopy* **87**, 97 (2001).
- <sup>3</sup>H. Sasaki *et al.*, *J. Electron Microsc.* **53**, 497 (2004).
- <sup>4</sup>M. H. F. Overwijk, F. C. van den Heuvel, and C. W. T. Bulle-Lieuwma, *J. Vac. Sci. Technol. B* **11**, 2021 (1993).
- <sup>5</sup>T. Ishitani, H. Tsuboi, T. Yaguchi, and H. Koike, *J. Electron Microsc.* **43**, 322 (1994), available at <http://jmicro.oxfordjournals.org/content/43/5/322.abstract>.
- <sup>6</sup>R. M. Langford and A. K. Petford-Long, *J. Vac. Sci. Technol. A* **19**, 2186 (2001).
- <sup>7</sup>J. Mayer, L. A. Giannuzzi, T. Kamino, and J. Michael, *MRS Bull.* **32**, 400 (2007).
- <sup>8</sup>N. I. Kato, *J. Electron Microsc.* **53**, 451 (2004).
- <sup>9</sup>B. B. Pate, *Surf. Sci.* **165**, 83 (1986).
- <sup>10</sup>J. Isberg, J. Hammersberg, E. Johansson, T. Wikström, D. J. Twitchen, A. J. Whitehead, S. E. Coe, and G. A. Scarsbrook, *Science* **297**, 1670 (2002).
- <sup>11</sup>W. Zhu, G. P. Kochanski, S. Jin, and L. Seibles, *J. Appl. Phys.* **78**, 2707 (1995).
- <sup>12</sup>L. Wei, P. K. Kuo, R. L. Thomas, T. R. Anthony, and W. F. Banholzer, *Phys. Rev. Lett.* **70**, 3764 (1993).
- <sup>13</sup>L. Tang, C. Tsai, W. W. Gerberich, L. Kruckeberg, and D. R. Kania, *Biomaterials* **16**, 483 (1995).
- <sup>14</sup>M. W. Geis, J. C. Twichell, and T. M. Lyszczarz, *J. Vac. Sci. Technol. B* **14**, 2060 (1996).
- <sup>15</sup>I. Aharonovich, A. D. Greentree, and S. Prawer, *Nature Photon.* **5**, 397 (2011).
- <sup>16</sup>J. R. Maze *et al.*, *Nature* **455**, 644 (2008).
- <sup>17</sup>F. C. Waldermann *et al.*, *Diam. Relat. Mater.* **16**, 1887 (2007).
- <sup>18</sup>A. Faraon, C. Santori, Z. Huang, V. M. Acosta, and R. G. Beausoleil, *Phys. Rev. Lett.* **109**, 033604 (2012).
- <sup>19</sup>T. M. Babinec, B. J. M. Hausmann, M. Khan, Y. Zhang, J. R. Maze, P. R. Hemmer, and M. Lončar, *Nature Nanotech.* **5**, 195 (2010).
- <sup>20</sup>J. Riedrich-Möller *et al.*, *Nature Nanotech.* **7**, 69 (2012).
- <sup>21</sup>P. Maletinsky, S. Hong, M. S. Grinolds, B. Hausmann, M. D. Lukin, R. L. Walsworth, M. Lončar, and A. Yacoby, *Nature Nanotech.* **7**, 320 (2012).
- <sup>22</sup>M. W. Doherty, N. B. Manson, P. Delaney, F. Jelezko, J. Wrachtrup, and L. C. L. Hollenberg, *Phys. Rep.* **528**, 1 (2013).
- <sup>23</sup>S. Pezzagna, D. Rogalla, D. Wildanger, J. Meijer, and A. Zaitsev, *New J. Phys.* **13**, 035024 (2011).
- <sup>24</sup>C. Wang, C. Kurtsiefer, H. Weinfurter, and B. Burchard, *J. Phys. B* **39**, 37 (2006).
- <sup>25</sup>J. R. Rabeau *et al.*, *Appl. Phys. Lett.* **88**, 023113 (2006).

- <sup>26</sup>J. Schwartz, P. Michaelides, C. D. Weis, and T. Schenkel, *New J. Phys.* **13**, 035022 (2011).
- <sup>27</sup>O. Gaathon, J. S. Hodges, E. H. Chen, L. Li, S. Bakhru, H. Bakhru, D. Englund, and R. M. Osgood, Jr., *Opt. Mater.* **35**, 361 (2013).
- <sup>28</sup>A. P. Magyar, J. C. Lee, A. M. Limarga, I. Aharonovich, F. Rol, D. R. Clarke, M. Huang, and E. L. Hu, *Appl. Phys. Lett.* **99**, 081913 (2011).
- <sup>29</sup>B. A. Fairchild *et al.*, *Adv. Mater.* **20**, 4793 (2008).
- <sup>30</sup>P. Olivero *et al.*, *Adv. Mater.* **17**, 2427 (2005).
- <sup>31</sup>D. P. Hickey, K. S. Jones, and R. G. Elliman, *Diam. Relat. Mater.* **18**, 1353 (2009).
- <sup>32</sup>B. A. Fairchild, S. Rubanov, D. W. M. Lau, M. Robinson, I. Suarez-Martinez, N. Marks, A. D. Greentree, D. McCulloch, and S. Praver, *Adv. Mater.* **24**, 2024 (2012).
- <sup>33</sup>D. P. Hickey, E. Kuryliw, K. Siebein, K. S. Jones, R. Chodelka, and R. Elliman, *J. Vac. Sci. Technol. A* **24**, 1302 (2006).
- <sup>34</sup>S. Rubanov and A. Suvorova, *Diam. Relat. Mater.* **20**, 1160 (2011).
- <sup>35</sup>W. R. McKenzie, Md. Z. Quadir, M. H. Gass, and P. R. Munroe, *Diam. Relat. Mater.* **20**, 1125 (2011).
- <sup>36</sup>M. V. Hauf *et al.*, *Phys. Rev. B* **83**, 081304 (2011).
- <sup>37</sup>B. Grotz *et al.*, *Nat. Commun.* **3**, 729 (2012).
- <sup>38</sup>S. Cui and E. L. Hu, e-print [arXiv:13041407](https://arxiv.org/abs/13041407) (2013).
- <sup>39</sup>J. Hodges, L. Li, E. Chen, M. Trusheim, S. Allegri, X. Yao, O. Gaathon, H. Bakhru, and D. Englund, *New J. Phys.* **14**, 093004 (2012).
- <sup>40</sup>B. J. M. Hausmann *et al.*, *Nano Lett.* **12**, 1578 (2012).
- <sup>41</sup>A. Faraon, C. Santori, Z. Huang, K. C. Fu, V. M. Acosta, D. Fattal, and R. G. Beausoleil, *New J. Phys.* **15**, 025010 (2013).
- <sup>42</sup>J. O. Orwa, K. W. Nugent, D. N. Jamieson, and S. Praver, *Phys. Rev. B* **62**, 5461 (2000).
- <sup>43</sup>S. A. Solin and A. K. Ramdas, *Phys. Rev. B* **1**, 1687 (1970).
- <sup>44</sup>V. Mochalin, S. Osswald, and Y. Gogotsi, *Chem. Mater.* **21**, 273 (2009).
- <sup>45</sup>V. Mochalin, O. Shenderova, D. Ho, and Y. Gogotsi, *Nature Nanotech.* **7**, 11 (2012).
- <sup>46</sup>A. C. Ferrari and J. Robertson, *Phil. Trans. R. Soc. Lond. A* **362**, 2477 (2004).
- <sup>47</sup>D. S. Knight and W. B. White, *J. Mater. Res.* **4**, 385 (1989).
- <sup>48</sup>A. E. Grigorescu and C. W. Hagen, *Nanotechnology* **20**, 292001 (2009).
- <sup>49</sup>J. Ziegler (2013), <http://www.srim.org>.
- <sup>50</sup>I. Bayn, A. Bolker, C. Cytermann, B. Meyler, V. Richter, J. Salzman, and R. Kalish, *Appl. Phys. Lett.* **99**, 183109 (2011).
- <sup>51</sup>I. Bayn *et al.*, *Diam. Relat. Mater.* **20**, 937 (2011).
- <sup>52</sup>I. Bayn, B. Meyler, J. Salzman, and R. Kalish, *New J. Phys.* **13**, 025018 (2011).